Jonathan Mamou, Michael L. Oelze,
William D. O'Brien, Jr., and James F. Zachary

Perspective on Biomedical Quantitative Ultrasound Imaging

Recent developments in ultrasonic imaging techniques involve the display of quantitative information. Quantitative ultrasound (QUS) has the potential to become a reliable, fast, and inexpensive technique to classify (diagnose) pathologies. The understanding of QUS images relies extensively on digital signal processing strategies. In our pilot studies, three types of tumors (rat fibroadenoma, mouse sarcoma, and mouse carcinoma) were investigated. QUS images that display average ultrasonic scatterer size and acoustic concentration were reconstructed from the processed in situ and calibrated backscattered ultrasound spectra. Furthermore, three-dimensional (3-D) tissue models were engineered from the histologic photomicrographs of these three tumors to generate tissue-based computational models. Comparison between the in vivo and computational phantom data of the same tissue has met with some success. However, to clinically realize this new technology, ultrasonic scattering in tissue must be fully understood and better interpreted using modern digital signal processing.

BACKGROUND

Conventional medical ultrasound B-mode images are constructed from envelope-detected radio frequency (RF) signals that are backscattered. The RF echoes are created by reflections from interfaces between acoustically different regions (macrostructure) and by coherent and incoherent scattering from tissue microstructures. B-mode image processing removes the frequency-dependent information available in the RF echo signals. Conventional B-mode images display large-scale structures (greater than wavelength), but to quantify spatially and display smaller scale structures (smaller than wavelength), the frequency-dependent echo data must be utilized.

To increase its competitiveness in the modern world of biomedical imaging and to provide medically meaningful images, ultrasound imaging needs to extend beyond qualitative B-mode imaging. To achieve this goal, quantitative and/or functional parameters must be pursued and appropriately displayed. The RF frequency-dependent ultrasound signals backscattered from biological tissues contain information about the size, shape, number, and relative impedance of the scattering objects within the tissues. Preliminary attempts to relate QUS scatterer property estimates to tissue microstructure identified from optical microscope images of the same tissues have had modest success [1].

The goal of this article is to introduce the signal processing community to the recent advances in the highly multidisciplinary field of QUS imaging. QUS relies heavily on signal processing techniques to extract information about underlying tissue microstructure. Our experience shows that digital signal processing is a significant component of our research and that modern signal processing strategies will enable us to continue to improve and refine QUS techniques.

DIGITAL SIGNAL PROCESSING AND QUANTITATIVE ULTRASOUND

QUS ESTIMATES FROM ULTRASONIC MEASUREMENTS

QUS estimates are made by parameterizing the in situ ultrasound backscattered power spectrum from a region-of-interest (ROI) of the interrogated tissue. Currently, models of scattering based on a 3-D spatial autocorrelation function (SAF) describing the shape and distribution of scatterers in the medium are used to extract the QUS parameters [2], [3]. By assuming that the scatterers have some internal impedance distribution and are spherical in shape, the SAF leads to closed-form solutions for the theoretical backscattered power spectrum

$$W_{\text{theor}}(f) = B(L, q)C(a_{\text{eff}}, n_z) \times f^4 F(f, a_{\text{eff}}), \qquad (1)$$

where f is the frequency (MHz) and C is a constant depending on the properties of the scatterers in the medium. These properties are the average effective radius a_{eff} of the scatterers (mm) and the average acoustic concentration (defined as the number density times the square of the fractional impedance change between scatterer and background) n_z of scatterers (mm^{-3}). The term $B(L, q)$ accounts for the source and windowing characteristics, where L is the length of the range gate and q is the ratio of the aperture radius to distance from the ROI. Finally, F is called the form factor (FF) and is a function of the frequency and average effective scatterer radius [2] and depends on the shape and mechanical properties of scatterers.

The FF describes the frequency dependence of scattering based on the size, shape, and mechanical properties of the scatterers. An important consideration for accurately estimating scatterer properties is the appropriate choice of the FF. The Gaussian FF has been used to model the scattering

1053-5888/06/$20.00©2006IEEE

properties of many soft tissues [2], [3]. The Gaussian FF represents a distribution of continuously changing impedance with the surrounding tissues, unlike a rigid or fluid-filled sphere that would represent an abrupt change with the surrounding soft tissue. Furthermore, the Gaussian scatterer has an effective radius related to the impedance distribution of the scatterer, unlike the definite radius describing a spherical shell or fluid-filled sphere. Use of the Gaussian FF and incorporation of the lateral and axial transducer beam characteristics into (1) leads to a theoretical power spectrum given by [3]

$$W_{\text{theor}}(f) = \frac{185 L q^2 a_{\text{eff}}^2 n_z f^4}{1 + 2.66\left(f q a_{\text{eff}}\right)^2} \times e^{-12.3 f^2 a_{\text{eff}}^2}. \quad (2)$$

Estimates of the scatterer properties are obtained [4] by equating the logarithm of the measured backscattered power spectrum averaged over the ROI to the logarithm of the theoretical power spectrum (2)

$$10\log\left[W_{\text{theor}}(f)\right] \approx 10\log(f^4) + m(a_{\text{eff}}, q) f^2 + b(n_z, a_{\text{eff}}, L, q). \quad (3)$$

Subtracting $10\log(f^4)$ from both sides of (3) and letting $x = f^2$ yields

$$10\log\left[W_{\text{theor}}(f)\right] - 10\log(x^2) \approx m(a_{\text{eff}}, q)x + b(n_z, a_{\text{eff}}, L, q). \quad (4)$$

Equation (4) describes a straight line where the slope m is a function of a_{eff} and q, and the intercept b is a function of a_{eff}, n_z, q, and L. The quantity q is determined by the characteristics of the operating transducer and L is known. To obtain the scatterer estimates, least-squares analysis is used to estimate the best-fit slope and intercept [4], [5]. Once the average effective scatterer radius is estimated from the slope of (4), the acoustic concentration is estimated from the intercept. Typically, values for the acoustic concentration span a large dynamic range; therefore, estimates of acoustic concentration are expressed on a decibel scale.

Prior to QUS processing, B-mode images were constructed from three kinds of tumors in rats and mice: a spontaneously growing mammary fibroadenoma in rats, a mouse mammary carcinoma, and a mouse mammary sarcoma. The rat tumors were scanned with a 10-MHz center-frequency transducer, and the mouse tumors were scanned with a 20-MHz center-frequency transducer. From the B-mode images, ROIs were selected from inside the tumors where the B-mode images appeared to be homogeneous (no interfaces or large echoes). The RF echo data were gated within each ROI using a sliding Hanning window with a 66% overlap. Each ROI is a square measuring 3 mm × 3 mm for the 10-MHz data and 1.5 mm × 1.5 mm for the 20-MHz data.

Scatterer property estimates are then determined for each ROI using the best-fit line estimation scheme for the Gaussian FF model (4) [4], [5]. Each ROI overlaps adjacent ROIs both laterally and axially by 66%. Pixel sizes are defined to be 1 mm × 1 mm and 0.5 mm × 0.5 mm for the 10-MHz and 20-MHz data, respectively. Each pixel is thus associated with scatterer property estimates averaged from corresponding, overlapping ROIs. The color of each pixel is assigned based on the value of the averaged scatterer property estimate associated with the pixel. The colored pixels are then superimposed on the gray-scale B-mode tumor images to create QUS images. Color bars, displayed with the QUS images, show the relationship between the colored pixels and the scatterer property estimates.

3-D ACOUSTIC MODELING OF TISSUE

To the best of our knowledge, the individual anatomical structures responsible for ultrasonic scattering in tissue have remained unidentified. Significant progress would be made if the complex interactions of ultrasound with tissue microstructures were better understood. One approach to better identify structures responsible for scattering is to engineer 3-D computational acoustic tissue models.

These models, termed 3-D impedance maps (3DZMs), are deduced from adjacent photomicrographs of stained histologic sections. The significance of these models is that the frequency-dependent information of the tissue microstructures can be estimated in a straightforward manner using frequency analysis techniques [6]. As a result, the same spectral parameters of interest (average scatterer size and acoustic concentration) can be obtained independently of the ultrasound backscattered estimates. In other words, the 3DZMs provide a tissue-based computational phantom that can be evaluated independently of ultrasound interrogation.

The tumor tissue is first scanned in vivo with ultrasound and spectral estimates are obtained following the methodologies described in the previous section. Following ultrasonic interrogation, the tumor is fixed in formalin, hematoxylin and eosin (H&E) stained, and sectioned (usually 3–5 μm). The adjacent sections are imaged and digitized (24-b bitmap) by a Nikon Optiphot-2 optical microscope and a Sony CCD-Iris/RGB color video camera. This dataset of histologic digital images has inherent artifacts that need to be addressed to reconstruct an accurate model.

The H&E stain uptake is generally different from one section to the next, leading to images with slightly different contrast. To guarantee the most similar contrast for every image in the histologic dataset, histogram equalization is conducted individually for each of the three color components (i.e., red, green, and blue) of each digitized image.

The alignment of the adjacent sections is suboptimal. Thus, after digitization and histogram equalization, the sections are aligned using an automatic nonrigid registration algorithm. This algorithm uses affine transforms [six degrees of freedom (DOFs), two

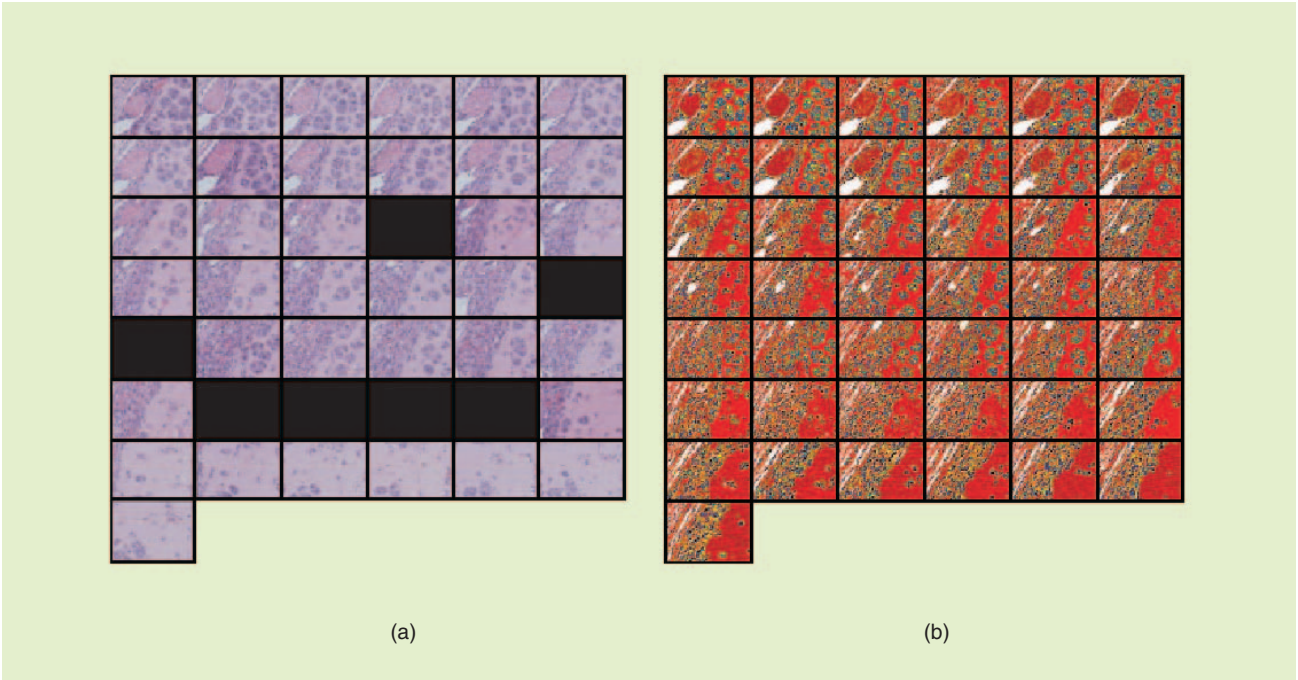

[FIG1] (a) A 43-section dataset from the sarcoma dataset. Sections are subimages of size 218 μm by 156 μm (i.e., 350 by 250 pixels) of the original 400 μm by 300 μm sarcoma. The sections were consecutive from left to right and top to bottom. Black fields symbolize the missing sections. (b) Contrast of the available sections was equalized. Each section was affine-registered with the next available section. Missing sections were Hermite-interpolated after equalization and after registration. A seven-level threshold algorithm was used to discriminate seven individual tissue constituents (represented by the seven arbitrary colors).

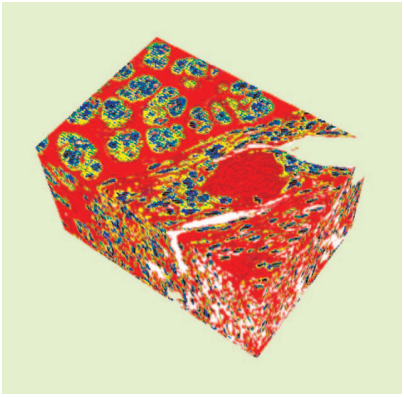

[FIG2] 3-D rendering of the 3DZM obtained from Figure 1. The rendered volume is of size 218 μm by 156 μm by 129 μm.

translational, one rotational, two stretching, and one shearing] to align each section with the next. The normalized mutual information (NMI) is used as a means to quantify similarity between images. The NMI approach makes use of entropy as defined in information theory and is computed from the histogram of each image and also the joint histogram of the two images being compared [7]

$$NMI(I, J) = \frac{H(I) + H(J)}{H(I, J)}, \qquad (5)$$

where $NMI(I, J)$ is the NMI value between images I and J and $H(I)$, $H(J)$, and $H(I, J)$ are the entropy of image I, the entropy of image J, and the joint-entropy between images I and J, respectively. This similarity measure has proven to be robust when compared to more conventional similarity measures (e.g., mean-squared difference or cross correlation). The optimal transform (i.e., the one that maximizes the NMI) is found by optimization using the simplex algorithm on the space of DOFs [8]. To limit the computational load during the optimization procedure, nearest-neighbor interpolation is conducted to interpolate the transformed images. Once the optimal transform is found, the image is reconstructed using a cubic interpolation kernel.

During tissue sectioning, a number of sections (~20%) are lost or destroyed. Thus, after alignment, the missing sections need to be interpolated. To interpolate the missing sections, cubic Hermite interpolating polynomials are used. Specifically, a third degree polynomial (four unknowns) has been found to match slope and values of the signals (images) on each side of a "hole." This process yields four equations from which the four unknowns are determined. The Hermite polynomials were chosen because they are shape-preserving, i.e., extrema present in the available data are also extrema in the reconstructed signal. This property is of particular interest when dealing with images because it guarantees that the reconstructed signals will still be in the 0–255 range, thus avoiding the need for postprocessing to compress values into the 0–255 range.

Finally, to convert each pixel value to an appropriate acoustic impedance value, a color-threshold algorithm is used on every H&E stained bitmap

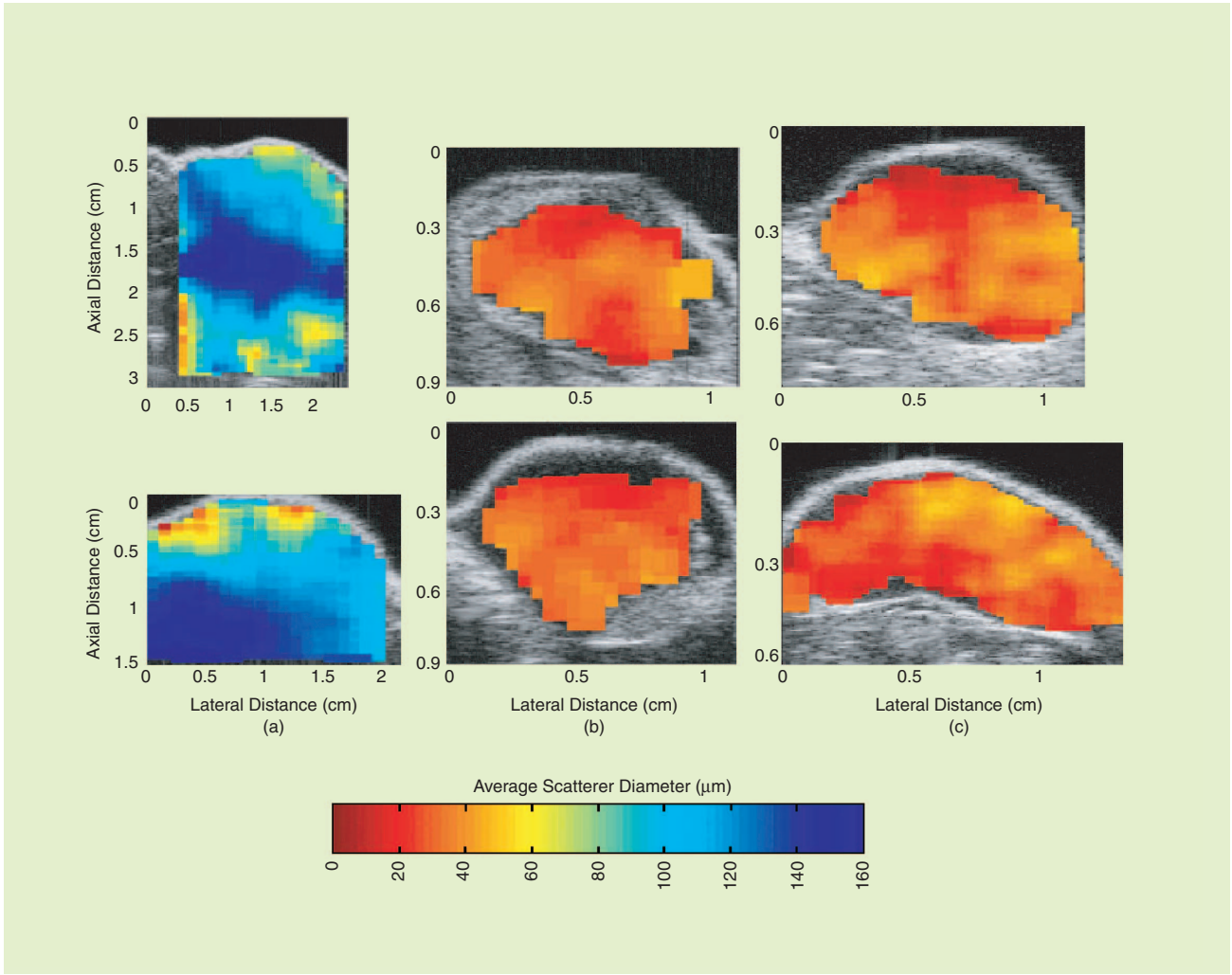

[FIG3] **Scatterer diameter images of three tumors: (a) fibroadenoma, (b) carcinomas, and (c) sarcomas.**

image. Tissue proteins stained with eosin yield shades of color ranging from very light pink to dark pink, depending on the concentration of protein within the structure. Nucleic acids stained with hematoxylin yield shades of color ranging from very light blue to dark blue, depending on the concentration of nucleic acid within the structure. This differential staining allows for the recognition of unique microstructures in the tissue. A range of colors corresponding to an identified microstructure in the stained bitmap images is then assigned a single color. The new single color is thus representative of the acoustic impedance value for that tissue microstructure. For each pixel of the same color in the color-thresholded bitmap image, the same acoustic impedance value is assigned. The design of the threshold algorithm was supervised by a board-certified pathologist. Figure 1, obtained from a mouse sarcoma, illustrates the complete reconstruction process. Figure 2 shows a 3-D rendering of the 3DZM of the mouse sarcoma.

To obtain spectral estimates, the Fourier transform of the spatial autocorrelation function (SAF) of the 3DZM is computed. Under plane wave incidence, Born approximation, and single scattering assumptions, the backscattered intensity (I_{bs}) can be deduced from this Fourier transform in a straightforward manner [9]

$$I_{bs} = Af^4 \left| \int\int\int \frac{z(r_0) - z_0}{z_0} e^{-2ikr_0} \mathrm{d}r_0 \right|^2, \tag{6}$$

where A is a proportionality constant, $z(r_0)$ is the acoustic impedance at location r_0, and z_0 is the acoustic impedance of the background. A Gaussian FF was chosen to model ultrasonic scattering because it is the FF used for the in situ ultrasonic evaluation of the tumors. The scatterer size and acoustic concentration are then estimated by fitting the Gaussian FF to the power spectrum of the 3DZM [6].

RESULTS

Figure 3 shows examples of scatterer diameter images of the three kinds of

[TABLE 1] SUMMARY OF ESTIMATES OBTAINED FROM TUMORS GROWN FROM THREE TUMOR CELL LINES.

	RAT FIBRAODENOMA	MOUSE CARCINOMA	MOUSE SARCOMA
IMPEDANCE VALUES USED (MRAYL)	1.58 – EPITHELIAL CELLS 1.54 – MAMMARY DUCT 1.80 – CONNECTIVE TISSUE	1.45 – FAT 1.58 – CYTOPLASM 1.60 – NUCLEI 1.60 – RED BLOOD CELLS 1.80 – CONNECTIVE TISSUE	2.00 – NUCLEAR HETEROCRHOMATIN 1.85 – NUCLEAR EUCHROMATIN 1.70/1.65 – EXTRACELLULAR MATRIX 1.60 – VASCULAR SPACE/BLOOD 1.58/1.55 – CYTOPLASM
3DZM SIZE (μm)	$800 \times 600 \times 390$	$200 \times 150 \times 330$	$218 \times 156 \times 129$
ULTRASOUND ESTIMATES	$<D> = 105 \pm 25\ \mu$m $<nz^2> = -15.6 \pm 5$ dB(mm^{-3})	$<D> = 30.0 \pm 9.6\ \mu$m $<nz^2> = 10.6 \pm 6.9$ dB(mm^{-3})	$<D> = 33 \pm 8.0\ \mu$m $<nz^2> = 9.9 \pm 5.3$ dB(mm^{-3})
3DZM ESTIMATES	$<D> = 91.5 \pm 25\ \mu$m $<nz^2> = -21.9 \pm 6.1$ dB(mm^{-3})	$<D> = 31.0 \pm 2.5\ \mu$m $<nz^2> = -1.4 \pm 6.1$ dB(mm^{-3})	$<D> = 32.9 \pm 6.1\ \mu$m $<nz^2> = -0.59 \pm 4.3$ dB(mm^{-3})

tumors that were ultrasonically scanned. Scatterer diameters were significantly larger for the fibroadenomas than for the carcinoma and sarcoma. However, estimates of the scatterer diameter using the Gaussian scatterer model did not reveal significant differences between the sarcoma and carcinoma.

Table 1 summarizes the results obtained for the three tumors. The estimates obtained using QUS and 3DZM methodologies are totally independent. The scatterer size estimates are very similar between the two independent techniques (within 10%). However, the acoustic concentration estimates obtained with the 3DZM are all significantly smaller than those obtained using QUS. More investigation is needed to fully understand these discrepancies. Nevertheless, the results are encouraging.

DISCUSSION AND CONCLUSIONS

QUS imaging displays quantitative information about tissue microstructure (subresolution). It is our hypothesis that this new class of images will provide significant diagnosis and disease-monitoring information.

However, what is needed for these new developments to become a routinely used imaging modality is a better understanding of what the ultrasonic estimates mean and how to relate them to pathologies. In our work, we proved that using the Gaussian FF, differences can be observed between the fibroadenomas and the other two types of tumors. However, it was not possible at this time to differentiate between the sarcoma and the carcinoma. One possible reason is the lack of specificity of the Gaussian FF to these tumors. In particular, it is worth mentioning that no tissue constituents would produce such a smooth impedance change; thus, considerable work is still required to determine the best FF.

To derive more tissue-specific FFs, our approach has been to acoustically model tissue in a 3-D fashion. It is our belief that if the 3DZMs are proved to be accurate acoustic representations of tumor tissues, then tissue-specific FF can be derived. The 3DZM approach provides the computational model from which signal processing strategies will be able to deduce appropriate tissue-specific FFs.

AUTHORS

Jonathan Mamou was with the Department of Electrical and Computer Engineering, University of Illinois at Urbana-Champaign. He is now with the Frederic L. Lizzi Center for Biomedical Engineering, Riverside Research Institute, New York. He can be contacted at mamou@rrinyc.org.

Michael L. Oelze is with the Department of Electrical and Computer Engineering and the Department of Bioengineering, University of Illinois at Urbana-Champaign.

William D. O'Brien, Jr. is with the Department of Electrical and Computer Engineering and the Department of Bioengineering, University of Illinois at Urbana-Champaign.

James F. Zachary is with the Department of Pathobiology and the Department of Bioengineering, University of Illinois at Urbana-Champaign.

REFERENCES

[1] R.C. Waag, J.O. Nilsson, and J.P. Astheimer, "Characterization of volume scattering power spectra in isotropic media from power spectra of scattering by planes," *J. Acoust. Soc. Amer.*, vol. 74, no. 5, pp. 1555–1571, 1983.

[2] M.F. Insana, R.F. Wagner, and D.G. Brown, "Describing small-scale structure in random media using pulse-echo ultrasound," *J. Acoust. Soc. Amer.*, vol. 87, no. 1, pp. 179–192, 1990.

[3] F.L. Lizzi, M. Astor, T. liu, C. Deng, D. Coleman, and R.H. Silverman, "Ultrasonic spectrum analysis for tissue assays and therapy evaluation," *Int. J. Imaging Syst. Technol.*, vol. 8, no. 1, pp. 3–10, 1997.

[4] M.L. Oelze, J.F. Zachary, and W.D. O'Brien, Jr., "Characterization of tissue microstructure using ultrasonic backscatter: Theory and technique for optimization using a Gaussian form factor," *J. Acoust. Soc. Amer.*, vol. 112, no. 3, pp. 1202–1211, 2002.

[5] M.L. Oelze, W.D. O'Brien, Jr., and J.F. Zachary, "Differentiation and characterization of rat mammary fibroadenomas and 4t1 mouse carcinomas using quantitative ultrasound imaging," *IEEE Trans. Med. Imaging*, vol. 23, no. 6, pp. 764–771, 2004.

[6] J. Mamou, M.L. Oelze, W.D. O'Brien, Jr., and J.F. Zachary, "Identifying ultrasonic scattering sites from 3D impedance maps," *J. Acoust. Soc. Amer.*, vol. 117, no. 1, pp. 413–423, 2005.

[7] C. Studholme, D.L.G. Hill, and D.J. Hawkes, "An overlap invariant entropy measure of 3D medical image alignment," *Pattern Recognit.*, vol. 32, no. 1, pp. 71–86, 1999.

[8] J.A. Nelder and R. Mead, "A simplex method for function minimization," *Computer J.*, vol. 7, no. 3, pp. 308–313, 1965.

[9] P.M. Morse and K.U. Ingard, *Theoretical Acoustics*. New York: McGraw-Hill, 1968. SP